Supporting Information

Maria Serral,[†] Marco Pinna,[‡] Andrei V. Zvelindovsky,[‡] and Josep Bonet Avalos[*,†]

Department d'Enginyeria Química, Universitat Rovira i Virgili, Tarragona, Av. dels Països Catalans, 26, 43007 Tarragona (Spain), and School of Mathematics and Physics, College of Science, University of Lincoln, Brayford Pool, Lincoln, Lincolnshire LN6 7TS, UK

E-mail: josep.bonet@urv.cat

Discussion on the thermal noise in CDS

Noise terms of the form $\zeta(\mathbf{r}, t)$ are often added[1,2] to the right hand side of eq 4, to induce thermal fluctuations, in the spirit of the fluctuating hydrodynamics of Landau and Lifshitz.[3] $\zeta(\mathbf{r}, t)$ is hence a Gaussian and white noise whose amplitude is determined by the Fluctuation-Dissipation theorem

$$\langle \zeta(\mathbf{r}, t)\, \zeta(\mathbf{r}', t') \rangle = 2M k_B T \nabla^2 \delta(\mathbf{r} - \mathbf{r}')\delta(t - t') \tag{S.1}$$

Two important features are directly related to the consideration of a noise term. On the one hand, the noise adds a scale of temperature in itself, in view of eq S.1. A phenomenological description given by a free-energy functional F similar to the used in this work (see eq 7) can contain the temperature entangled with the model parameters, due to the coarse-grained nature (see the comments in the paragraph below eq 8). In the presence of noise terms it is

---

[*]To whom correspondence should be addressed
[†]Universitat Rovira i Virgili
[‡]University of Lincoln

customary to consider the parameters in eq 7 as tunable and the temperature in eq S.1 as the physical scale of temperature.[4–7] On the other hand, one has to realize that the system's free-energy functional is no longer F if the noise is present. F then takes the role of a *potential of mean force*. The equilibrium of the system is no longer determined by the minimum of F but of some related functional renormalized by the noise.

The dynamics described in the manuscript hence corresponds to a system with a macroscopic order paramenter with negligible thermal fluctuations. Using standard arguments, this implies that if n is the total number of monomers in a unit cell of size d^3, the relative weight of the fluctuations scales as $\langle \delta n^2 \rangle / \langle n \rangle^2 \simeq \langle n \rangle^{-1}$. Hence, the larger the number of monomers inside the unit cell, the less important will be the thermal fluctuations, provided that we are far from the critical point. Therefore, since the size of the unit cell is proportional to $N^{2/3}$ in the strong seggregation limit, large polymers will comply with this condition.

Although in the numerical implementation of the relaxation represented by eq 4 we add a random term for numerical convenience, this term has no physical meaning, neither the dynamics generated. The noise term complies with the condition of conservation of Ψ. Only the final equilibrium state with the noise amplitude set to zero represents the minimum of the free energy F we are seeking. The noise in our work is therefore a computational tool used to overcome local energy barriers.

Qualitative analysis of the system

To have an intuitive idea about the meaning of the parameters that we use in the simulations, let us address here a qualitative analysis.

The extremes of $H[\Psi]$ in eq 8 are given by

$$\Psi^0 = 0 \tag{S.2}$$

$$\Psi^\pm = -\frac{v(1-2f)}{2u} \pm \sqrt{\left(\frac{v(1-2f)}{2u}\right)^2 - \frac{\tau'}{u}} \tag{S.3}$$

2

Hence, the critical point is given by $\tau'_c = v^2(1 - 2f)^2/4u$, where the second term in eq S.3 vanishes. If $\tau' < \tau'_c$, the two roots in eq S.3 are real and correspond to two minima of $H[\Psi]$. The third root $\Psi = 0$ corresponds to a maximum. Instead, if $\tau > \tau'_c$, only one real solution $\Psi = 0$ exists, which corresponds to a minimum. Approximately, the values of $\Psi^\pm$ set the relative volume occupied by each block, due to the order parameter conservation and that the integral of Ψ over the volume is zero. Hence, due to this latter fact, it has to be further required that $\tau' < 0$ to have $\Psi^+ > 0$, which is the only situation with physical meaning for the problem formulated by eq 7. We consider that $\tau' < 0$ from now on. For some of the values of τ' the fields $\Psi^\pm$ are not in agreement with eq 5. This is a drawback of the used mapping function, which should be interpreted as an expansion for small Ψ of a more complex H, in the spirit of the Ginzburg-Landau theory. However, the the free-energy functional is still physically meaningful and therefore, the simulation results are qualitatively significant. Although one could not extract precise values of the volume fractions of each block from Ψ, the field indicates the separation between A-rich regions Ψ^- from B-rich regions Ψ^+.

Secondly, if $\tau' < 0$ the system separates into the aforementioned $A-$ and $B-$rich regions, which take characteristic form and size. Let us consider that the system forms spheres which distribute in space in an ordered structure with a unit cell, whose lateral size d characterizes the distance between spheres. The volume of such unit cell is of the order of d^3, since prefactors are ignored along the analysis. Hence, the conservation of the order parameter implies

$$m\frac{4\pi}{3}R_s^3\Psi^+ - \left(L^3 - m\frac{4\pi}{3}R_s^3\right)|\Psi^-| \sim 0 \tag{S.4}$$

where m is the number of cells in the system and L^3 is the total volume. Hence,

$$m \sim \frac{L^3}{d^3} \tag{S.5}$$

Therefore,

$$R_s \sim d\,\rho^{1/3} \tag{S.6}$$

3

where we have introduced the parameter

$$\rho \equiv \left(\frac{|\Psi^-|}{\Psi^+ + |\Psi^-|} \right) \tag{S.7}$$

Therefore, the relative size of the domains of each block are determined not only by the characteristic size of the cell d, but also by the values taken by $\Psi^{\pm}$.

The scaling of the lateral dimension of the cell as well as the characteristic size of the Ψ^+ region in the model parameters is determined by the balance between the interface F_s and connectivity F_{lr} free-energy terms, since the effect of the mapping function is to cause the phase separation into two bulk phases. Thus,

$$F_s[\Psi(\mathbf{r})] + F_{lr}[\Psi(\mathbf{r})] = \int d\mathbf{r} \left\{ \frac{D}{2} |\nabla \Psi|^2 + \frac{B}{2} \int d\mathbf{r}' G(\mathbf{r} - \mathbf{r}') \Psi(\mathbf{r}) \Psi(\mathbf{r}') \right\} \tag{S.8}$$

In the strong segregation limit[8] the interface thickness between Ψ^+ and Ψ^-, namely ξ, is much smaller than the polymer size. Thus, we can derive the scaling form of the first term F_s

$$\int d\mathbf{r} \frac{D}{2} |\nabla \Psi|^2 \sim D \frac{\Psi^2}{\xi^2} \xi R_s^2 m \sim DL^3 \frac{\Psi^2}{\xi} \frac{\rho^{2/3}}{d} \tag{S.9}$$

where use has been made of the fact that the integrand is of the order of Ψ^2/ξ^2 and is only different from zero in the volume occupied by the interfacial region $\xi R_s^2 m = \xi R_s^2 L^3/d^3$. Eqs S.5 and S.6 are also used in the last similarity. On the other hand, the second term in eq S.8 scales as

$$\frac{B}{2} \int d\mathbf{r} \int d\mathbf{r}' G(\mathbf{r} - \mathbf{r}') \Psi(\mathbf{r}) \Psi(\mathbf{r}') \sim BL^3 \frac{\Psi^2}{d} d^3 \sim BL^3 \Psi^2 d^2 \tag{S.10}$$

where we have assumed that the outer integral is of the order of L^3 and that the inner integral of the propagator is of the order of $(\Psi^2/d) \times d^3$, since beyond d the alternation of Ψ makes its contribution to the inner integral very small. Such scaling form is independent of whether the geometry is spherical, cylindrical or lamellar, since the inner integral is dominated by

the shortest distance due to the $1/r$-dependence of the integrand. Hence, using in eq S.8 the scaling forms of the surface and long-range contributions given, respectively, in eqs S.9 and S.10, yields

$$F \sim DL^3 \frac{\Psi^2}{\xi} \frac{\rho^\nu}{d} + BL^3\Psi^2 d^2 \tag{S.11}$$

with $\nu = 2/3$ for spheres. Minimizing this last equation with respect to d, one can estimate that the characteristic distance between structures scales as

$$d \sim \left(\frac{D\rho^{2/3}}{B\xi} \right)^{1/3} \equiv d_0 \rho^{2/9} \tag{S.12}$$

The last equality is a definition of d_0 to highlight the dependence in ρ. Since $B \sim N^{-2}$, according to eq 12, we recover the scaling $d \sim N^{2/3}$ of Ohta and Kawasaki,[8] as well as the dependence in the interfacial thickness. The weak segregation limit can be recovered by realizing that the surface contribution scales as $B\Psi^2 L^3/d^2$ since the interfacial thickness is $\xi \sim d$ itself. Thus, in this latter case we also recover the scaling form for the weak segregation limit[9] $d \sim (D\rho^{2/3}/B)^{1/4} \sim N^{1/2}$. We only consider the strong segregation limit from now on.

Repeating the calculation but assuming that the system arranges in parallel cylinders, one also finds an estimate of the radius R_c of the cylinder $R_c \sim d\rho^{1/2}$, and the exponent $\nu = 1/3$. d is found to scale as

$$d \sim \left(\frac{D\rho^{1/2}}{B\xi} \right)^{1/3} = d_0 \rho^{1/6} \tag{S.13}$$

Similarly, lamellae thickness is given by the relation $R_l \sim d\rho$ and $\nu = 0$. Then

$$d \sim \left(\frac{D}{B\xi} \right)^{1/3} = d_0 \tag{S.14}$$

Notice that the scaling law $N^{2/3}$ is the same as for the spherical case for both cylinders and lamellae.[8]

The scaling analysis cannot predict the relative stability of the different structures, which can be found in,[8] due to the importance of the neglected prefactors. However, inserting the obtained scaling forms of d, given in eqs S.12, S.13, and S.14 into the scaling form of the free energy, one obtains

$$F \sim \Psi^2 L^3 B d_0^2 \, \rho^\mu \tag{S.15}$$

with $\mu = 4/9 \simeq 0.44$, for spheres, $\mu = 1/3 \simeq 0.33$ for cylinders and $\mu = 0$ for lamellae. Hence, the value of the exponent μ indicates that low values of ρ favor the formation of spheres, while values close to 1 produce lamellae, with a transition to cylinders in between. Although the analysis is qualitative, it gives an idea about the role played by the parameters of the model under study. These results are in agreement with the detailed analysis of the phase diagram done by Ohta and Kawasaki.[8] Moreover, eq S.15 also qualitatively explains why within our model and parameters annealing produces cylinders early in the evolution while quenching produces directly spheres.

Euclidean distance between structures

In order to perform a quantitative analysis of the obtained structures, we introduce an Euclidean distance between the local environment of spheres and two relevant patterns for our system. Focusing on the 2-D arrangements, these ideal patterns are the hexagonal (HEX) arrangement and a (110) plane of a body-centered cube (BCC) distribution. In Figure 1 we sketch two layers of spheres arranged according to these two structures

To evaluate such a Euclidean distance, we proceed as follows. For each sphere we identify its center and the ones of its 6 nearest-neighbors within the same plane, parallel to the surface, and containing the center of the former (within a tolerance of 4 lattice spacings, corresponding to a half sphere radius up and down its center). To locate these centers we have used a method based on a large collection of code-vectors, which dynamically move down the gradient of Ψ to cluster around the points of low $\Psi \simeq \Psi^-$. Then, a clustering
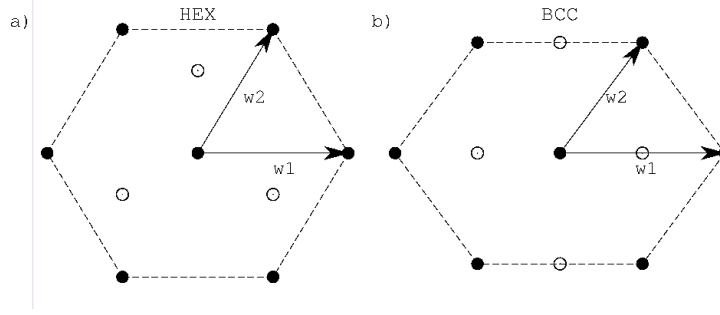
Figure 1: Characteristic distribution of spheres; a) hexagonal symetry, b) (110) plane of a BCC symetry. The central sphere with the six coplanar nearest-neighbors are represented by filled circles while the nearest neighbors of the layer behind are represented by open circles.

identification based on the closeness of the code-vectors permits to discriminate the code-vectors belonging to each domain and assign a centroid to it. Cylinders on the bottom wall are excluded.

The positions of the 6 neighbors' centers with respect to the central sphere's center define a 18-dimensional vector $\mathbf{v}$ describing the local structure of the central domain. The distance between two of these structures, namely $\mathbf{v} = (\mathbf{v}_1, \mathbf{v}_2, \ldots, \mathbf{v}_6)$ and $\mathbf{a} = (\mathbf{a}_1, \mathbf{a}_2, \ldots, \mathbf{a}_6)$, is simply defined as

$$\Delta^2(\mathbf{v}, \mathbf{a}) = \sum_{k=1}^{6} {}' \sum_{\alpha=x,y,z} \left(v_{\alpha,perm(k)} - a_{\alpha,k} \right)^2 \tag{S.16}$$

The prime stands for the fact that a given ordering of the vectors of one of the structures (say $\mathbf{v}$) is implied. The ordering is defined by simultaneously rotating the six 3-D vectors of $\mathbf{v}$ until $\mathbf{v}_1$ is parallel to $\mathbf{a}_1$. Then, we calculate all permutations of the identifiers of the remaining vectors $perm(k)$, to compare with the set $\mathbf{a} = (\mathbf{a}_1, \mathbf{a}_2, \ldots, \mathbf{a}_6)$, which contains a fixed ordering of the vectors. We further calculate $\Delta_{perm(k)}$ for each permutation. We repeat the operation rotating again the initial structure but now aligning $\mathbf{v}_2$ with $\mathbf{a}_1$ and calculating the permutations of all remaining vectors and the associated distances. After the rotation of all six vectors, Δ is taken as the minimum of all the calculated Δ's. This procedure is intended to remove any bias in the identification of who is who when comparing two structures.

The norm of $\mathbf{v}$ is defined as

$$||\mathbf{v}||^2 \equiv \sum_{k=1}^{6} \sum_{\alpha=x,y,z} v_\alpha^2 \tag{S.17}$$

To calculate the distance according to eq S.16, $\mathbf{v}$ has been previously normalized such that $||\mathbf{v}|| = \sqrt{6}$, which is the norm of the HEX and BCC patterns as we have defined them in Table 1.

A pattern is thus also defined as a 18-dimensional vector whose norm, from eq S.17 is taken to be 6 by definition. The two planar patterns considered are defined by the six positions given in Figure 1.

Hence, the distance between the obtained local structure and the HEX (or BCC) pattern is calculated as $\Delta(\mathbf{v}, \mathbf{w})$ where the vectors $\mathbf{w}$ defining the pattern are given in Table 1.

Table 1: Characteristic vectors defining a hexagonal arrangement (HEX) and a (110) plane of a body-centered cubic (BCC) arrangement. $\mathcal{N}$ is the norm of the 18-dimensional vector, according to eq S.17, divided by $\sqrt{6}$. For the HEX $\mathcal{N} = 1$, while for the BCC $\mathcal{N} = \sqrt{5/6}$

	HEX			BCC		
	x	y	z	x	y	z
$a_1\mathcal{N}$	1	0	0	1	0	0
$a_2\mathcal{N}$	1/2	$\sqrt{3}/2$	0	1/2	$1/\sqrt{2}$	0
$a_3\mathcal{N}$	$-1/2$	$\sqrt{3}/2$	0	$-1/2$	$1/\sqrt{2}$	0
$a_4\mathcal{N}$	-1	0	0	-1	0	0
$a_5\mathcal{N}$	$-1/2$	$-\sqrt{3}/2$	0	$-1/2$	$-1/\sqrt{2}$	0
$a_6\mathcal{N}$	1/2	$-\sqrt{3}/2$	0	1/2	$-1/\sqrt{2}$	0

References

(1) Chen, L. Q.; Shen, J. *Computer Physics Communications* **1998**, *108*, 147.

(2) Hamley, I. W. *Macromol. Theory Simul.* **2000**, *9*, 363.

(3) Landau, L. D.; Lifshitz, E. M. *Fluid Mechanics*; Pergamon Press: London, 1958.

(4) Zvelindovsky A.V., Z. A. *Il Nuovo Cimento D* **1997**, *19*, 725–745.

(5) van Vlimmeren, B. A. C.; Maurits, N. M.; Zvelindovsky, A. V.; Sevink, G. J. A.; Fraaije, J. G. E. M. *Macromolecules* **1999**, *32*, 646–656.

(6) Knoll, A.; Lyakhova, K. S.; Horvat, A.; Krausch, G.; Sevink, G. J. A.; Zvelindovsky, A. V.; Magerle, R. *Nature Materials* **2004**, *3*, 886–890.

(7) Horvat, A.; Sevink, G. J. A.; Zvelindovsky, A. V.; Krekhov, A.; Tsarkova, L. *ACS Nano* **2008**, *2*, 1143–1152.

(8) Ohta, T.; Kawasaki, K. *Macromolecules* **1986**, *19*, 2621.

(9) Leibler, L. *Macromolecules* **1980**, *13*, 1602.